CrossMark

Monitoring cotton (*Gossypium hirsutum* L.) germination using ultrahigh-resolution UAS images

Ruizhi Chen[1] · Tianxing Chu[2] · Juan A. Landivar[3] · Chenghai Yang[4] · Murilo M. Maeda[3]

Abstract Examination of seed germination rate is of great importance for growers early in the season to determine the necessity for replanting their fields. The objective of this study was to explore the potential of using unmanned aircraft system (UAS)-based visible-band images to monitor and quantify the cotton germination process. A light-weight UAS platform was used, which carried a consumer-grade red, green, and blue camera stabilized by a built-in gimbal system. In order to obtain ultrahigh image resolution during the germination stage, the UAS platform was flown at an altitude of approximately 15–20 m above ground. By applying the structure-from-motion (SfM) algorithm, the images were rectified and orthographically mosaicked with a ground sampling distance of approximately 6–9 mm/pixel. A novel solution was then developed for calculating the average plant size and the number of germinated cotton plants according to the leaf polygons extracted from the orthomosaic images. By using the estimated number of germinated cotton plants, the plant density and the cumulative germination rate can also be estimated in a straightforward manner using field-specific parameters. An assessment of the proposed solution was conducted by comparing the estimated number of the germinated cotton plants against ground observation data collected from six cotton row segments. The results demonstrated that the average estimation accuracy achieved 88.6% in terms of identifying the number of the germinated cotton plants. The accuracy may be further improved if images with near infrared band are employed.

✉ Tianxing Chu
   tianxing.chu@tamucc.edu

[1] State Key Laboratory of Information Engineering in Surveying, Mapping and Remote Sensing, Wuhan University, No.129 Luoyu Rd., Wuhan 430079, Hubei, China

[2] Conrad Blucher Institute for Surveying and Science, Texas A&M University Corpus Christi, 6300 Ocean Dr., Corpus Christi, TX 78412, USA

[3] Texas A&M AgriLife Research and Extension Center, 10345 TX-44, Corpus Christi, TX 78406, USA

[4] USDA-Agricultural Research Service, 3103 F&B Road, College Station, TX 77845, USA

Introduction

Seed germination is the most significant stage for stand establishment, and includes complex interactions such as water absorption, membrane reorganization, metabolic restructuring, and cell expansion (Hake et al. 1990). During seed germination, it is of great importance for the growers to be able to monitor the germination and stand establishment processes as early as possible so they can determine the need to replant their fields in a timely manner, if plant density is not adequate.

Studies on cotton germination have been extensively conducted in controlled laboratory environment. Most studies in the past focused on quantifying seed germination rates by varying soil temperature to find out (1) the optimal temperature range for germination, and (2) the germination temperature tolerance range. Research shows that soil temperatures below 20 °C tend to slow germination rates (Lehman 1925; Krzyzanowski and Delouche 2011) while optimum germination happens at temperatures above 20 °C to around 34 °C (Toole and Drumond 1924; Lehman 1925; Camp and Walker 1927; Arndt 1945; Cole and Wheeler 1974).

Outside of the controlled laboratory environment, airborne and satellite remote sensing has been widely acknowledged as an effective technology to assess crop growth status. Commercial satellite imagery vendors can provide well-tuned products over large spatial and temporal scales; however, spatial and temporal resolutions from satellite imagery are often inadequate, especially during crop germination and emergence stages. Airborne remote sensing, on the other hand, is capable of improving observation resolutions in a more flexible manner.

Until recently, extensive agricultural studies have used multirotor and fixed-wing unmanned aircraft system (UAS) platforms to carry various types of miniaturized sensors to effectively perform crop monitoring tasks under a variety of circumstances (Gevaert et al. 2015; Rasmussen et al. 2013; Zhang and Kovacs 2012). It has been demonstrated that UAS platforms offer a unique opportunity to develop a variety of precision agriculture applications with the focus on assessing crop growth, vegetation and health status (Berni et al. 2009; Honkavaara et al. 2013; Li et al. 2012; López-Granados et al. 2016). The versatility and flexibility of UAS platforms allow convenient and cost-effective access to customized spatial, temporal, and even spectral resolutions (Colomina and Molina 2014). Nevertheless, after an exhaustive literature review, there is no previous study that aimed at investigating the use of UAS photogrammetry as a tool for crop germination assessment.

The objective of this work was to introduce a novel solution for monitoring and quantifying the cotton germination process based on ultrahigh-resolution red, green, and blue (RGB) imagery obtained from a low-cost UAS platform. The main contributions of this study are twofold. First, this work pioneered a comprehensive methodology and workflow to investigate the potential of quantifying cotton germination using a UAS platform. Low-altitude UAS imagery with a high revisit frequency enables us to perform reliable assessments based on a large number of small-size seedling samples with adequate temporal and spatial resolutions. Second, this research was carried out in the field instead of a laboratory environment. As stated above, previously published germination research

papers focused on controlled environments; whereas, this study lifted the environment restriction and assessed the proposed solution by comparing against more than two thousand ground observation samples.

Materials and methods

Study area

The 85 m × 54 m study area was established at the Texas A&M AgriLife Research and Extension Center (27° 46.948′ N, 97° 33.605′ W) at Corpus Christi, TX, as shown in Fig. 1. The blue paddle in the left subfigure indicates the geolocation of the study area in relation to the city of Corpus Christi, Texas, and the test field details are revealed in the right subfigure. A total of 35 cotton varieties were planted at a rate of 13.3 seeds/m in the test field on April 1, 2015. The test field was separated into seven 10.67 m-long segments, in north–south direction. Each segment consisted of 56 rows spaced at 0.96 m. Each variety plot consisted of two consecutive rows in each segment. As shown in Fig. 1, each variety was replicated four times as indicated by different colors. Border plots delineated with translucent cerulean color depict filler rows in each segment and were excluded from analysis in this study. In the test field discussed in this paper, cotton emergence was observed on April 6, 2015, and the cotton was harvested on August 17, 2015. It is worth noting that the background orthographic image of the test field used in Fig. 1 was generated from UAS images taken on June 26, 2015.

Data collection

Imagery collection from UAS platform

Operating a light-weight UAS is as simple as pushing a button on the smartphone after planning the flight mission. The UAS platform for this research was a Phantom 2 Vision+ multirotor copter (DJI, Shenzhen, Guangdong, China). A DJI Phantom Vision
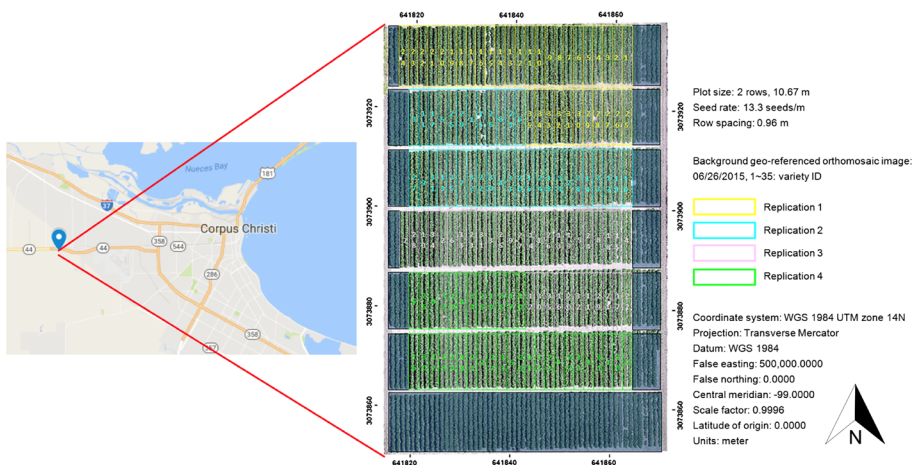
Fig. 1 Test field at the Texas A&M AgriLife Research and Extension Center in Corpus Christi, TX

FC200 RGB camera was mounted on the UAS platform. With robust UAS gimbal support, stabilized nadir camera observation to the field was enabled. Some key features of the images taken by the camera are provided in Table 1. Common camera settings, such as white balance, ISO sensitivity, and exposure time, were kept on automatic or default mode to minimize experiment complexity.

During the cotton germination stage, UAS images were acquired on a per day basis starting from April 7, 2015 [i.e. 6 days after planting (DAP)] and ending on April 12, 2015 (i.e. 11 DAP). Due to non-technical reasons, the image data were not properly collected on April 8, 2015 (i.e. 7 DAP) and therefore were excluded from subsequent analysis. The UAS was flown at an altitude of 15–20 m above ground in order to achieve favorable image ground sampling distance (GSD) for clearly observing germination of small-size cotton cotyledons and leaves. An average horizontal speed of 1 m/s was configured and the camera snapped a shot once the UAS traveled 1 m horizontally to obtain sufficient along-track and across-track overlaps for generating orthomosaic images of the whole test field. The flight time for each experiment was about 20 min to cover the whole test field. The images for each flight experiment were captured around local noon so as to optimize the homogeneity of light intensity and reflectance for a fair assessment for all datasets. Table 2 shows the number of images captured, GSD of the orthomosaic image as well as the flight altitude above ground for each day during the germination stage.

Routine flight experiments were conducted on a weekly or biweekly basis afterwards until early harvest stage, depending on the local weather conditions. A complete-cycle analysis of cotton growth modeling and assessment for the same test field has been published earlier by Chu et al. (2016).

Ground control points

Four ground control points (GCPs) were established at corners of the test field to georeference the orthomosaic images. They ensured that the orthomosaic images have a unified geodetic scale under the same coordinate system. The GCPs were surveyed using an Altus APS-3 receiver (Altus Positioning Systems, Torrance, CA, USA) with the Texas Department of Transportation (TxDOT) virtual reference station (VRS) positioning solution that can offer a positioning accuracy up to a few centimeters. Table 3 lists the coordinates of the four GCPs installed at the corners of the test field under the World Geodetic System 1984 (WGS-84).

Table 1 Key features of the images taken by the DJI Phantom Vision FC200 RGB camera

Image features	
Array	4608 × 3456 pixels
Sensor size	6.17 mm × 4.55 mm
Focal length	5.0 mm
White balance	Auto
Exposure time	1/1250
ISO sensitivity	100
Bits per sample	8
Image format	JPEG

Table 2 Summary of UAS flight experiments during the germination stage (i.e. April 7–12, 2015)

DAP[a]	Number of images	GSD of the orthomosaic image (mm/pixel)	Flight altitude above ground (m)
6	159	8.86	20
8	225	8.90	20
9	155	8.91	20
10	180	6.58	15
11	187	6.31	15

[a] Image data were not properly collected on April 8, 2015 (i.e. 7 DAP)

Table 3 The geodetic coordinates of the GCPs under the WGS-84 coordinate system

| GCP No.	Latitude ($^\circ$)	Longitude ($^\circ$)	Height (m)
1	27.781689	−97.560620	−11.08
2	27.781699	−97.560067	−11.13
3	27.782471	−97.560075	−10.96
4	27.782466	−97.560629	−11.00

Ground germination data collection

While most industry-level germination equipment, such as germinator and seed container, is mainly utilized for laboratory analytics, this UAS-based research, however, strived for monitoring cotton germination process at the open field. As a cost- and time-effective alternative, a Samsung Galaxy Note 3 smartphone (Samsung, Suwon, South Korea) was employed to collect in situ germination data by recording videos along the cotton row segments. Ground germination data was collected on April 12, 2015 (i.e. 11 DAP). To record a live video along a selected cotton row, the smartphone was held at a height of 0.5 m above ground. The ground data collector meanwhile walked slowly along the row with an average moving speed of 0.6 m/s. After evaluating the ground-based workload and complexity, three entire rows (i.e. tenth, 20th, and 30th rows) were selected for video collection out of 56 total cotton rows (including filler rows). As the length of each row segment was 10.67 m in average, a total of $6 \times 3 \times 10.67 = 192.06$ m-long cotton rows were sampled as ground-collected germination data. The number of cotton plants for each selected row was manually counted by playing back the video in the laboratory. A total of 2077 cotton plant samples were ground truthed from these three selected rows. Compared with previous works which primarily focused on laboratory germination analytics, this study has extensively enlarged the number of ground truthed germination samples used for assessment. Figure 2 shows an example of a frame of the live video that was used to count the total number of germinated cotton plants.

Meteorological data collection

Temperature has a strong influence on cotton seed germination rate and therefore a meteorological station was installed on the northwest corner of the test field to measure air temperature, relative humidity as well as soil temperature. Table 4 shows the meteorological data of the test field during the germination stage. Air temperature ranged from 21.8

Fig. 2 Example of a video frame used for counting the number of germinated cotton plants
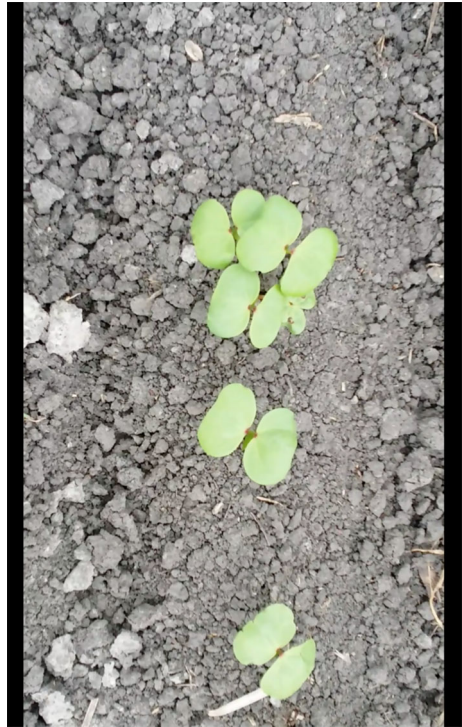
Table 4 Meteorological data measured at the test field during the germination stage

DAP	Relative humidity (%)	Air temp. (°C)	Soil temp. (°C)[a]	Soil temp. (°C)[b]	Daily heat unit[c]	Cumulative heat units after planting
6	85.1	24.4	26.7	25.8	18.4	90.6
8	86.4	24.8	27.2	26.7	18.4	127.6
9	100	21.9	23.8	24.3	11.3	138.8
10	99.6	21.8	23.3	23.3	12.1	150.9
11	91.1	23.5	25.1	24.6	14.1	164.9
Average	92.4	23.3	25.2	24.9	14.9	–

[a] Soil temperature at the depth of 25.4 mm

[b] Soil temperature at the depth of 76.2 mm

[c] Degree days base 60F (DD60)'s heat unit with the threshold temperature of 60F (15.6 °C)

to 24.8 °C while soil temperature at 25.4 mm depth ranged from 23.3 to 27.2 °C. Relative humidity was greater than 85% throughout the period studied (Table 4).

Data processing

Figure 3 shows the diagram of the data processing procedure of the proposed germination analysis solution. There are four main steps:
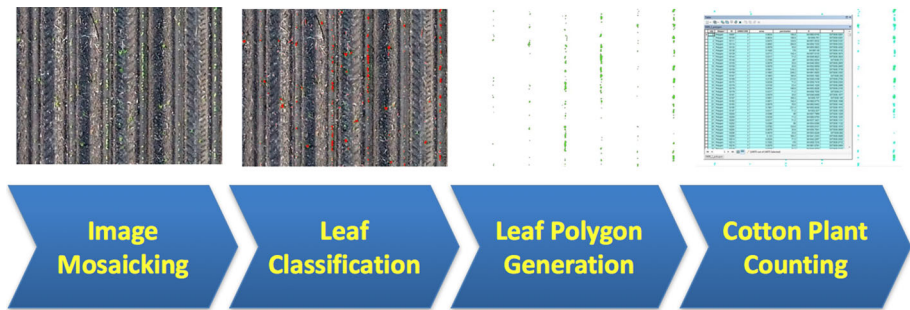
Fig. 3 Diagram of the proposed cotton germination analysis solution using RGB images obtained from the light-weight UAS platform

1) geo-referencing and mosaicking raw images taken from the UAS platform to create orthomosaic images for the whole test field,
2) classifying the orthomosaic images into two categories: cotton leaves and non-leaf objects,
3) generating the cotton leaf polygons based on the classified orthomosaic images, and
4) removing noise and counting the number of germinated cotton plants according to the number and size of the leaf polygons.

Orthomosaic image generation

The raw images were loaded in and processed by the Pix4Dmapper Pro (Pix4D SA, 1015 Lausanne, Switzerland) software after acquisition. The software applies the scale-invariant feature transform (SIFT) (Lowe 2004), or similar descriptor algorithm, to find key points and match a large number of images. The matching process geometrically determines the projection of a pair of matched points in different images representing the same 3D object. The software then utilizes the photogrammetric structure-from-motion (SfM) algorithm (Hartley and Zisserman 2004) to access high-resolution 3D first-surface-return point cloud and 2D orthomosaic image by stitching together common features between overlapping images.

A 3D first-surface-return point cloud model is usually used to estimate plant height (Bendig et al. 2015; Chu et al. 2016; Zarco-Tejada et al. 2014) or 3D plantation dimensionality (Díaz-Varela et al. 2015; Gatziolis et al. 2015; Torres-Sánchez et al. 2015), while a georeferenced 2D orthomosaic image provides a uniform scale and geometrically corrected view over the entire test field, facilitating applications such as crop disease and damage detection (Di Gennaro et al. 2016; Garcia-Ruiz et al. 2013; Yang and Hoffmann 2015). In this study, 3D plant point clouds were excluded from analysis due to the ignorable height of cotton seedlings compared with surrounding soil, and 2D orthomosaic images were primarily used for monitoring the germination process.

Cotton leaf classification

In order to monitor and quantify the germination process, cotton leaves were first identified and extracted from the orthomosaic images. In each orthomosaic image of the test field, all objects were classified into two categories: leaf and non-leaf objects. After manually training a few samples on each category, an interactive supervised maximum likelihood

classifier (Settle and Briggs 1987) was used for classifying the leaf and non-leaf objects in the ArcMap 10.3.1 (Esri, Redlands, CA, USA) software. Figure 4(a) shows an example of the classification results. In Fig. 4(a), green polygons indicate objects classified as cotton leaves. However, as seen in the rectangular areas inside the magnifier window, weeds in between two adjacent rows were also identified as cotton plants. Discriminating between weeds and cotton leaves by color is difficult as they both had green leaves in RGB images. Furthermore, at times some small cotton cotyledons were also classified as non-leaf objects because their color was similar to the dry plant residues on the field as shown in the circled area inside the magnifier window in Fig. 4(a).

Leaf polygon generation

In this step plants classified as cotton leaves were converted into a map layer of polygons using the ArcMap 10.3.1 software. The shape of the leaf polygon varied depending on (1) the size of the cotton leaves of a single plant, and (2) the number of plants in a cluster where leaves of the neighboring cotton plants were overlapped. In this study, the following geometric properties of each polygon were calculated:

– area of the polygon, and
– 2D coordinates of the centroid of the polygon.

The polygon areas were used to estimate the total number of germinated cotton plants, while the 2D coordinates of the centroids of the polygons were used to remove the weeds

Fig. 4 Example of the cotton leaf classification and leaf polygon generation

growing between planted cotton rows. As discussed above, there were other plants such as weeds growing between planted cotton rows. During this step, an off-the-line filter was designed to examine whether the centroid point of a polygon area classified as leaves was crossed by a cotton row line. The filter removed any plants that appeared off the cotton rows, while retaining plants roughly located on a cotton row line. Any weeds germinating along the cotton rows were considered as 'miscounted' cotton plants.

Figure 4(b) shows an example area of the leaf polygons generated from the leaf classification results. It also shows that the weeds were filtered out based on their location relative to the cotton rows. After excluding filler rows as illustrated in Figs. 1, 4(c) displays 16 628 leaf polygons in total in the entire map layer on April 12, 2015 (i.e. 11 DAP).

Germination statistics

The total number of germinated cotton plants was estimated based on the following three factors:

- the average plant size in terms of leaf area,
- the total number of leaf polygons, and.
- the area of each leaf polygon.

Therefore, three processing steps were introduced in this step:

- noise filtering: among all leaf polygons created in the above subsection, at times there were some small-size noise polygons generated by fresh plant residues. Inclusion of these noise polygons can lead to an overestimate of the total number of leaf polygons, and hence reduce the accuracy of estimating the total number of germinated cotton plants. In order to exclude those noise polygons induced by fresh plant residues, the area threshold of a leaf polygon was defined as $4p^2$ ($2p \times 2p$) mm^2, where p represents the average GSD of the orthomosaic image. Any polygon with an area less than this threshold was considered as noise, which was consequently removed from the map layer of polygons. Again, during this step, most of the weeds were already removed by clipping out the corresponding polygons outside of the cotton rows.
- estimate of the average plant size: After filtering out the noise and weed polygons, the average plant size s was estimated with.

$$s_j = \frac{\sum_{i=1}^{n} a_i}{n} \quad 4p^2 \leq a_i \leq T_j \tag{1}$$

where T_j indicates the threshold of the maximum size of a single cotton plant for the j-th DAP, a_i represents the area of the i-th single-plant leaf polygon among the complete number of n. All polygons that met the selection criterion $4p^2 \leq a_i \leq T_j$ shown in Eq. (1) were considered as single-plant leaf polygons.

- counting the numbers of leaf polygons that were classified into different categories based on their sizes. According to the aforementioned discussion, a leaf polygon may not contain a single plant, but multiple neighboring cotton plants that overlapping leaves. In order to accurately estimate the total number of germinated cotton plants, leaf polygons were classified into six categories, which assumes a leaf polygon may contain one, two, three, four, five or six cotton plants. A leaf polygon that may contain seven or more cotton plants were not considered in this study. The leaf polygon classification criteria are listed in Table 5. It is worth noting that, according to Eq. (1),

the average plant size s expands with DAP, while the leaf polygon classification criteria remain the same during the germination stage.

According to the above hypothesis in Table 5, the number of total germinated cotton plants m was then estimated with.

$$m = \sum\nolimits_{k=1}^{6} k \cdot G_k \qquad (2)$$

where G_k is the number of leaf polygons of the k-th category as depicted in Table 5. The plant density was then estimated with.

$$d = \frac{r \cdot m}{L} \qquad (3)$$

where r is the row length per 1/1000 ac (4.21 m), L is the total length of cotton rows (2996.0 m). The cumulative germination rate g was estimated with.

$$g = \frac{m}{A} \qquad (4)$$

where A is the number of total cotton seeds planted in the test field. In this study case, $A = 39\,847$ as the seed rate was 13.3 seeds/m.

Results

Daily average plant size

The daily average plant size was estimated according to Eq. (1) during the germination stage. It is an average leaf area of a single cotton plant. The value of this parameter increased with DAP as a result of the growth of the cotton plants. Table 6 lists the estimated average plant size s over DAP and its corresponding parameters used for the estimation. A linear growing trend of the average plant size over the whole test field is revealed in Fig. 5(a) where R^2 = coefficient of determination of the linear regression. The average plant size s was then used to define the classification threshold of the leaf polygons as listed in Table 5.

Germination statistical results

By comparing the area of each leaf polygon with the threshold parameters obtained in Table 5, the number of leaf polygons for each size category G_k was determined. The daily
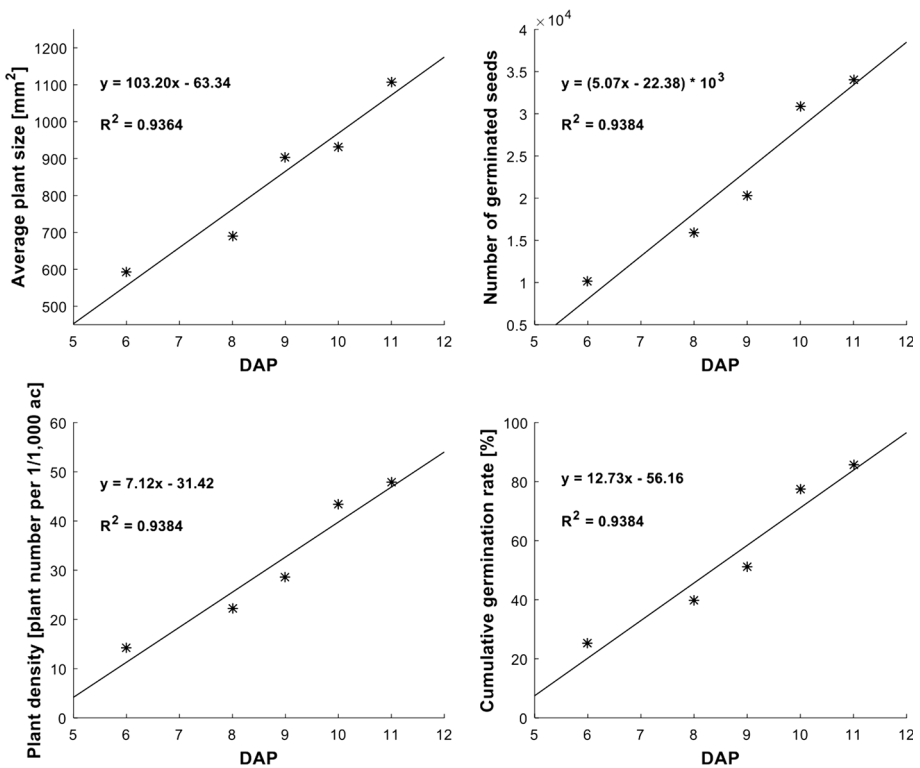
Table 5 Leaf polygon classification criteria	Leaf polygon categories		Classification criteria	
	Category No.	Description	Minimum (mm^2)	Maximum (mm^2)
	1	1 plant	$4p^2$	$2s$
	2	2 plants	$2s$	$3s$
	3	3 plants	$3s$	$4s$
	4	4 plants	$4s$	$5s$
	5	5 plants	$5s$	$6s$
p average GSD	6	6 plants	$6s$	–
s average plant size				

Table 6 The estimated average plant size over DAP and its corresponding parameters used for the estimation

DAP	GSD p (mm/pixel)	Threshold of maximum plant size T (mm^2)	Estimated average plant size s (mm^2)	Number of leaf polygons used n
6	8.9	1200.0	591.6	2514
8	8.9	1600.0	689.8	5405
9	8.9	1800.0	903.9	5774
10	6.6	2000.0	931.2	8106
11	6.3	2200.0	1108.0	10 231

Fig. 5 Time series of cotton germination statistics estimated from the proposed UAS-based imagery solution over the whole test field. **a** Daily average plant size; **b** total number of germinated cotton seeds; **c** estimated plant density (measured as the number of plants per 1/1000 ac); **d** daily cumulative germination rate

total number of germinated cotton plants m was then estimated according to Eq. (2) based on G_k and the polygon size k. Furthermore, Eqs. (3) and (4), were used to estimate the plant density d and the cumulative germination rate g. Figure 5(b) shows the cumulative numbers of germinated cotton plants across DAPs. Figure 5(c) illustrates the time series in terms of the plant density, which represents a measure of the number of plants per 1/1000 ac. Figure 5(d) depicts the cumulative germination rate over DAP. It is clear that all the

statistical variables in Fig. 5 fit well with DAP in an increasing linear trend, producing R^2 values higher than 0.90. It is worth noting that the discrete values and linear regressions in Fig. 5(b–d) differ in scale and unit; however, they display the same ascending pattern over DAP with the same R^2 value. This is because, according to Eqs. (3) and (4), proportional linear relationships exist among Fig. 5(b–d). Table 7 summarizes the statistical details of the daily average plant size, number of total germinated cotton seeds, plant density, and cumulative germination rate over the whole test field during the germination stage by using the proposed estimation solution.

In this study, in addition to the estimated cumulative germination rate obtained from the open field, results obtained from the laboratory environment were also listed for discussion. As the average soil temperature (25.4 mm depth) of the test field during the germination stage was 25.2 °C as listed in Table 4, the laboratory results with soil temperature of 26 °C were used for comparison (Krzyzanowski and Delouche 2011). Detailed statistical results are listed in Table 8 where "days after emergence (DAE)" is used as the first column instead of "DAP" in order to match the terminology used by Krzyzanowski and Delouche (2011). Specifically, as emergence was first observed on April 6, 2015 in the test field, the DAE numbers in Table 8 correspond to the DAP numbers in Tables 2, 4, 6 and 7, respectively. According to Table 8, the cotton seeds germination rate in the controlled laboratory environment increased much faster than in the open field environment though the final germination rates were similar. For the laboratory environment, regardless of the seed type, most cotton seeds germinated within three days under soil temperature of 26 °C, while the germination process in the open field more or less followed a linear trend in terms of the average plant size and the number of total germinated seeds as shown in Figs. 5(a, b). This probably relates to the fact that in the laboratory environment, key biotic and abiotic factors that affect cotton seed germination and seedling establishment remained consistent and/or maximum control, which may not always be the case in a field environment.

Performance assessment

In order to validate the performance of the proposed cotton germination solution developed in this study, the estimated number of cotton plants derived from the UAS-based imagery was compared with the ground observation data. Figure 6 illustrates where the ground observation data was collected and how it was segmented for the validation procedure. The background map layer was from UAS imagery captured on April 9, 2015 (i.e. 8 DAP). The

Table 7 Summary of the daily average plant size, number of total germinated cotton seeds, plant density, and cumulative germination rate over the whole test field during the germination stage by using the proposed estimation solution

DAP	Estimated average plant size (mm^2)	Total number of germinated cotton seeds	Plant density (plant number per 1/1000 ac)	Cumulative germination rate (%)
6	591.6	10 122	14.21	25.4
8	689.8	15 850	22.25	39.8
9	903.9	20 372	28.60	51.1
10	931.2	30 865	43.33	77.5
11	1108.0	34 081	47.85	85.5

Table 8 Comparison of the cumulative germination rates between the results obtained from the test field and the laboratory environment (Krzyzanowski and Delouche 2011)

Days after emergence (DAE)	Field (%)	Lab-H (%)[a]	Lab-M (%)[b]
1	25.4	67.5	52.5
3	39.8	88.8	71.3
4	51.1	90.0	75.0
5	77.5	91.3	75.0
6	85.5	91.3	75.0

[a] *Lab-H* with high quality seeds

[b] *Lab-M* with low quality seeds

three rows (i.e. tenth, 20th and 30th rows from left to right) encompassed by the red rectangles represent the ground observation video data collected using the Samsung Galaxy Note 3 smartphone. There were 2077 cotton plant samples observed in a total of 192.06 m of row.

The performance assessment was divided into six segments. Each segment cropped 10.67 m of the field in length, and therefore examined the estimated number of cotton plants against the ground observation. In contrast with the background image as shown in Figs. 1, 6 ignored the seventh segment which consisted of filler (also known as border) cotton seeds planted on the south-most side of the test field. Table 9 displays the accuracy comparison between the estimated number of germinated cotton plants in each selected row segment against the corresponding ground truth. When taking into account all six segments, the estimation accuracy ranged from 81.0% to 99.5% with an average of 88.6% in terms of counting germinated cotton plants.

Moreover, it is seen in Table 9 that for most segments (except for segment 1) the estimated numbers of cotton plants are smaller than the ground observed numbers. One of the major error sources in the proposed solution stemmed from non-green color reflectance of some small cotyledons in the RGB images. This directly led to errors in cotton leaf classification and thus an underestimate of the total number of germinated seeds. To address this problem, images from a multi-spectral or near-infrared (NIR) camera can be added to further improve discrimination between plant and non-plant objects in the field.

Summary and discussion

A UAS-based visual-band imagery solution has been developed in this study to monitor and quantify the cotton germination process. The light-weight UAS platform carried a consumer-grade RGB camera stabilized by an integrated onboard gimbal system. The built-in GPS module was used to adjust flight position and speed according to the flight command information and to write geotags to the images. In order to obtain an ultrahigh spatial resolution during the germination stage, the UAS platform was flown at an altitude of approximately 15–20 m above ground. Images were captured at a rate of 1 image/s with a planned horizontal ground speed of 1m/s to fulfill 70 and 60% overlap between images along- and across-track, respectively. Consecutive RGB images with 4608×3456 pixels were captured and stored in the onboard SD card with JPEG format. Common camera settings were kept on automatic or default mode to minimize experiment complexity.
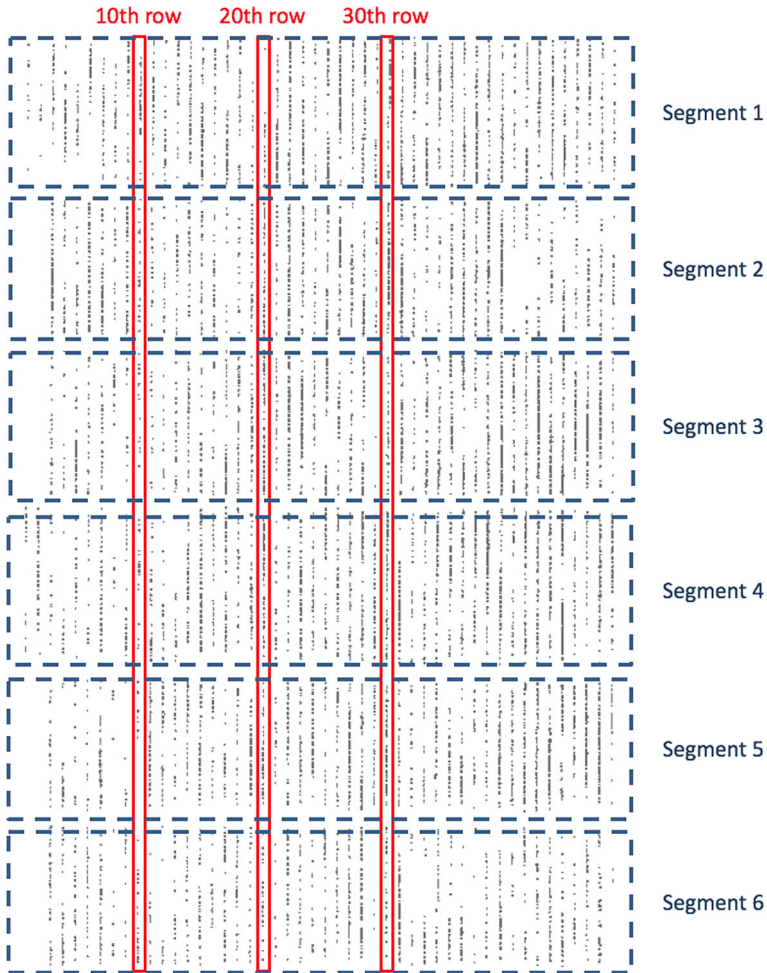
Fig. 6 Illustration of the ground observation data and segments on the cotton test field

The ultrahigh-resolution images can be loaded into available geospatial computing software (e.g. Pix4Dmapper Pro and Agisoft PhotoScan Professional) to generate 2D (orthomosaic images) and 3D (point clouds) products according to the SfM algorithm. In this study case, the orthomosaic images achieved a GSD of 6–9 mm/pixel. Therefore, during the germination stage cotton plants were identifiable against soil using a supervised classification strategy, available in remote sensing software (e.g. ArcGIS and ERDAS IMAGINE). By extracting the leaf polygons from the orthomosaic images, the proposed solution has demonstrated that UAS-based RGB imagery is capable of assessing quantitatively the number of germinated cotton plants, estimating the plant density, and calculating the cumulative germination rate during the germination stage. The performance of the proposed solution was assessed by comparing the ground observation data from 2077 cotton plant samples, and an average accuracy of 88.6% was confirmed.

To the best of the authors' knowledge, there is no previous research investigating the process of crop germination in an open field environment utilizing UAS platforms. The

Table 9 Accuracy comparison between the estimated number of germinated cotton plants in each selected row segment against ground truth

Segment	Number of estimated germinated cotton plants	Number of cotton plants obtained from ground observation	Accuracy (%)
1	407	405	99.5
2	280	317	88.3
3	345	369	93.5
4	304	367	82.8
5	284	329	86.3
6	235	290	81.0
Average			88.6

methodology proposed here opens the door for germination-related research and quite possibly future precision agriculture applications. Results in this study confirm that UAS platforms have great potential for precisely monitoring cotton germination, which may help cotton growers obtain accurate information early in the season for effective and timely management decisions.

The total hardware cost for this study was approximately $1300 US dollars, and included platform, camera, gimbal system, and remote controller. A smartphone or laptop computer was also needed for displaying real-time flight statistics and/or for pre-planning the flight mission. One can select a more advanced imaging or UAS platform which may provide refined spatial and/or spectral resolution. The use of geospatial computing software for image processing, however, requires additional user costs and geomatics knowledge, thus may limit the rapid adoption of UAS imagery-based tools among crop growers. Therefore, to achieve specific goals in a timely and cost-effective manner, collaborative work among crop growers and agricultural solution providers or geospatial computing scientists would be favorable at this time. A big advantage of UAS-based precision agriculture is that agricultural fields extend across large and open-sky areas, and therefore flight operations are usually under minimized restrictions in terms of safety and privacy issues that have largely hindered the UAS uses in populated urban areas. The UAS platforms could help scout a disease at an early growth stage or enhance routine management practices such as irrigation scheduling, fertilization, and pesticide application. Recent study has discovered that by properly using UAS technology in crop scouting, an estimated $1.3 billion return on investment (ROI) could be reached annually for corn, soybean and wheat growers nationwide in the United States in terms of increasing crop yields and reducing input costs (AFBF 2015; USDA 2015).

The use of NIR images is a popular way to further improve RGB observations for effective crop vegetation monitoring. Although high accuracy results may be achieved, Table 9 also reveals that the proposed methodology may underestimate the number of the germinated plants due to new cotyledons' non-green color reflectance captured by a visual-band camera lens. In order to further improve the identification performance, an additional pre-aligned camera with high sensitivity and spatial resolution at the NIR band is recommended to reduce the probability of errors. As an alternative, by applying filtering techniques, one can use a single standard RGB camera to access both NIR and color bands to expand the applicability of this work (Yang and Hoffmann 2015).

Nowadays, in the United States, public agencies or institutions usually need to apply for the Certificates of Waiver or Authorization (COA) to gain airspace access from the Federal Aviation Administration (FAA) for UAS operations. The FAA must balance societal and economic benefits of commercial UAS industry against broader issues of public safety and national security. Despite regulatory limitations being a major challenge for UAS-based applications, the FAA has been continuously taking steps to allow for more convenience and flexibility to industry, government and academic UAS operators for various applications. For instance, blanket COA has recently allowed UAS operators with section 333 Exemption to conduct flights up to 121.92 m altitude (FAA 2016a). More recently, a new waiver program under Part 107 has been announced, and it provided a new path for flight permission as a possibly easier alternative to the section 333 Exemption (FAA 2016b). With the release of the new regulatory rules, agricultural UAS opportunity for commercial and institutional uses is expected to be greatly expanded, and approximately 80 percent of the domestic UAS market is anticipated coming from agriculture and related industries (Jenkins and Vasigh 2013).

References

AFBF. (2015). Fact sheet: quantifying the benefits of drones in precision agriculture. American Farm Bureau Federation. Retrieved January 31, 2017 from http://www.measure.aero/wp-content/uploads/2015/07/AFBF-Fact-Sheet.pdf.

Arndt, C. H. (1945). Temperature-growth relations of the roots and hypocotyls of cotton seedlings. *Plant Physiology, 20*(2), 200–220.

Bendig, J., Yu, K., Aasen, H., Bolten, A., Bennertz, S., Broscheit, J., et al. (2015). Combining UAV-based plant height from crop surface models, visible, and near infrared vegetation indices for biomass monitoring in barley. *International Journal of Applied Earth Observation and Geoinformation, 39,* 79–87.

Berni, J. A. J., Zarco-Tejada, P. J., Suárez, L., & Fereres, E. (2009). Thermal and narrowband multispectral remote sensing for vegetation monitoring from an unmanned aerial vehicle. *IEEE Transactions on Geoscience and Remote Sensing, 47*(3), 722–738.

Camp, A. F., & Walker, M. N. (1927). Soil temperature studies with cotton. II. The relation of soil temperature to germination and growth of cotton. *Florida Agricultural Experimental Station Bulletin, 189,* 17–32.

Chu, T., Chen, R., Landivar, J. A., Maeda, M. M., Yang, C., & Starek, M. J. (2016). Cotton growth modeling and assessment using unmanned aircraft system visual-band imagery. *Journal of Applied Remote Sensing, 10*(3), 036018.

Cole, D. F., & Wheeler, J. E. (1974). Effect of pregermination treatments on germination and growth of cotton seed at sub-optimal temperatures. *Corp Science, 14*(3), 451–454.

Colomina, I., & Molina, P. (2014). Unmanned aerial systems for photogrammetry and remote sensing: a review. *ISPRS Journal of Photogrammetry and Remote Sensing, 92,* 79–97.

Di Gennaro, S. F., Battiston, E., Di Marco, S., Facini, O., Matese, A., Nocentini, M., et al. (2016). Unmanned aerial vehicle (UAV)-based remote sensing to monitor grapevine leaf stripe disease within a vineyard affected by esca complex. *Phytopathologia Mediterranea, 55*(2), 262–275.

Díaz-Varela, R. A., de la Rosa, R., León, L., & Zarco-Tejada, P. J. (2015). High-resolution airborne UAV imagery to assess olive tree crown parameters using 3D photo reconstruction: application in breeding trials. *Remote Sensing, 7*(4), 4213–4232.

FAA. (2016a). FAA Form 7711-1 UAS COA: Blanket COA for any operator issued a valid Section 333 grant of exemption. Federal Aviation Administration of the United States. Retrieved November 1, 2016

from https://www.faa.gov/uas/beyond_the_basics/section_333/how_to_file_a_petition/media/Section-333-Blanket-400-COA-Effective.pdf.

FAA. (2016b). Fact Sheet – Small Unmanned Aircraft Regulations (Part 107). Federal Aviation Administration of the United States. Retrieved November 9, 2016 from https://www.faa.gov/news/fact_sheets/news_story.cfm?newsId=20516.

Garcia-Ruiz, F., Sankaran, S., Maja, J. M., Lee, W. S., Rasmussen, J., & Ehsani, R. (2013). Comparison of two aerial imaging platforms for identification of Huanglongbing-infected citrus trees. *Computers and Electronics in Agriculture, 91,* 106–115.

Gatziolis, D., Lienard, J. F., Vogs, A., & Strigul, N. S. (2015). 3D tree dimensionality assessment using photogrammetry and small unmanned aerial vehicles. *PLoS ONE, 10*(9), e0137765.

Gevaert, C. M., Suomalainen, J., Tang, J., & Kooistra, L. (2015). Generation of spectral–temporal response surfaces by combining multispectral satellite and hyperspectral UAV imagery for precision agriculture applications. *IEEE Journal of Selected Topics in Applied Earth Observations and Remote Sensing, 8*(6), 3140–3146.

Hake, K., McCarty, W., Hopper, N., Jividen, G. (1990). Seed quality and germination. Cotton Physiology Today–Newsletter of the Cotton Physiology Education Program. National Cotton Council. Retrieved November 1, 2016 from http://www.cotton.org/tech/physiology/cpt/variety/upload/CPT-Mar90-REPOP.pdf.

Hartley, R., & Zisserman, A. (2004). *Multiple view geometry in computer vision* (2nd ed.). Cambridge, UK: Cambridge University Press.

Honkavaara, E., Saari, H., Kaivosoja, J., Pölönen, I., Hakala, T., Litkey, P., et al. (2013). Processing and assessment of spectrometric, stereoscopic imagery collected using a lightweight UAV spectral camera for precision agriculture. *Remote Sensing, 5*(10), 5006–5039.

Jenkins, D., Vasigh, B. (2013). The economic impact of unmanned aircraft systems integration in the United States. Association for Unmanned Vehicle Systems International. Retrieved January 31, 2017 from http://www.auvsi.org/econreport.

Krzyzanowski, F. C., & Delouche, J. C. (2011). Germination of cotton seed in relation to temperature. *Revista Brasileira de Sementes., 33*(3), 543–548.

Lehman, S. G. (1925). Studies on treatment of cottonseed. *North Caroline Agricultural Experimental Station, 26,* 1–71.

Li, X., Lee, W. S., Li, M., Ehsani, R., Mishra, A. R., Yang, C., et al. (2012). Spectral difference analysis and airborne imaging classification for citrus greening infected trees. *Computers and Electronics in Agriculture, 83,* 32–46.

López-Granados, F., Torres-Sánchez, J., Serrano-Pérez, A., de Castro, A., Mesas-Carrascosa, F., & Peña, J. (2016). Early season weed mapping in sunflower using UAV technology: variability of herbicide treatment maps against weed thresholds. *Precision Agriculture, 17*(2), 183–199.

Lowe, D. G. (2004). Distinctive image features from scale-invariant keypoints. *International Journal of Computer Vision, 60*(2), 91–110.

Rasmussen, J., Nielsen, J., Garcia-Ruiz, F., Christensen, S., & Streibig, J. C. (2013). Potential uses of small unmanned aircraft systems (UAS) in weed research. *Weed Research, 53*(4), 242–248.

Settle, J. J., & Briggs, S. S. (1987). Fast maximum likelihood classification of remotely sensed imagery. *International Journal of Remote Sensing, 8*(5), 723–734.

Toole, E. H., & Drumond, P. L. (1924). The germination of cotton seed. *Journal Agricultural Research, 28*(3), 285–295.

Torres-Sánchez, J., López-Granados, F., Serrano, N., Arquero, O., & Peña, J. M. (2015). High-throughput 3-D monitoring of agricultural-tree plantations with unmanned aerial vehicle (UAV) technology. *PLoS ONE, 10*(6), e0130479.

USDA. (2015). Acreage (June 2015). National Agricultural Statistics Service, United States Department of Agriculture. Retrieved January 31, 2017 from https://www.usda.gov/nass/PUBS/TODAYRPT/acrg0615.pdf.

Yang, C., & Hoffmann, W. C. (2015). Low-cost single-camera imaging system for aerial applicators. *Journal of Applied Remote Sensing, 9*(1), 096064.

Zarco-Tejada, P. J., Diaz-Varela, R., Angileri, V., & Loudjani, P. (2014). Tree height quantification using very high resolution imagery acquired from an unmanned aerial vehicle (UAV) and automatic 3D photo-reconstruction methods. *European Journal of Agronomy, 55,* 89–99.

Zhang, C., & Kovacs, J. M. (2012). The applications of small unmanned aerial systems for precision agriculture: a review. *Precision Agriculture, 13*(6), 693–712.